

Large animal model of acute right ventricular failure with functional tricuspid regurgitation



Marcin Malinowski^{a,b,1}, Alistair G. Proudfoot^{a,1}, Lenora Eberhart^{a,1}, Hans Schubert^{a,1}, Jeremy Wodarek^{a,1}, David Langholz^{a,1}, Manuel K. Rausch^{c,1}, Tomasz A. Timek^{a,*,1}

^a Meijer Heart and Vascular Institute at Spectrum Health, 100 Michigan Ave NE, Grand Rapids, MI 49503, USA

^b Department of Cardiac Surgery, Medical University of Silesia, School of Medicine in Katowice, Ziolowa 47, 40635 Katowice, Poland

^c Department of Aerospace Engineering & Engineering Mechanics, Department of Biomedical Engineering, Institute for Computational Engineering and Science, University of Texas at Austin, 210 E 24th Street, Austin, TX 78703, USA

ARTICLE INFO

Article history:

Received 15 January 2018

Received in revised form 12 February 2018

Accepted 19 February 2018

Keywords:

Right ventricular failure

Tricuspid regurgitation

Strain

Tricuspid valve

Right ventricle

ABSTRACT

Background: Functional tricuspid regurgitation (FTR) commonly arises secondary to conditions affecting the left heart and is associated with right ventricular dysfunction and tricuspid annular dilatation. We set out to establish an animal model of acute RV failure (RVF) with FTR resembling the clinical features.

Methods: Ten adult sheep had pressure sensors placed in the LV, RV, and right atrium while sonomicrometry crystals were implanted around tricuspid annulus and on the RV. Animals were studied open-chest to assess for RV function and FTR after: (1) volume infusion, (2) pulmonary artery constriction, (3) 5 min posterior descending artery occlusion, and (4) combination of all interventions. Hemodynamic, echocardiographic, and sonomicrometry data were collected at baseline and after every intervention. RV dimensions, RV strain, and annular area, perimeter, and size were calculated from crystal coordinates. The model was validated in six additional sheep studied only before and after combined interventions.

Results: Neither volume infusion, pulmonary hypertension, nor ischemia were associated with RVF or clinically significant TR when applied separately but combined resulted in RVF and greater than moderate FTR. In the validation group, maximal RV volume increased (62 ± 14 vs 70 ± 16 ml, $p = 0.006$), contractility decreased (20 ± 6 vs $12 \pm 2\%$, $p = 0.02$), and strain increased. FTR increased from 0.4 ± 0.5 to 2.5 ± 0.8 ($p < 0.001$) and annular area from 652 ± 87 mm² to 739 ± 87 mm² ($p = 0.005$).

Conclusions: The developed ovine model of acute RVF was associated with significant annular and RV enlargement and FTR. This novel and clinically pertinent research platform offers insight into the acute RVF pathophysiology and can be utilized to evaluate treatment interventions.

© 2018 Elsevier B.V. All rights reserved.

1. Introduction

Right ventricular failure (RVF) is a situation when the ventricle is unable to adequately pump blood to the lungs and maintain proper left ventricular at low filling pressures. Its most common cause is left sided heart failure and pulmonary hypertension [1]. Right ventricular dysfunction is associated with increased morbidity and mortality in both the general population and patients undergoing cardiac surgery

Abbreviations: CPB, cardiopulmonary bypass; CVP, central venous pressure; EDP, end-diastolic pressure; FTR, functional tricuspid regurgitation; HR, heart rate; LV, left ventricle; PDA, posterior descending artery; PHT, pulmonary hypertension; RA, right atrium; RV, right ventricle; TR, tricuspid regurgitation.

* Corresponding author at: Meijer Heart and Vascular Institute at Spectrum Health, 100 Michigan Ave SE, Grand Rapids, MI 49503, USA.

E-mail address: Tomasz.Timek@spectrumhealth.org (T.A. Timek).

¹ These authors take responsibility for all aspects of the reliability and freedom from bias of the data presented and their discussed interpretation.

[2,3]. This clinical condition is often accompanied by significant tricuspid regurgitation. Functional (or secondary) tricuspid regurgitation (FTR) observed in these patients is not related to intrinsic damage of the valve but is the result of valvular complex remodeling characterized predominantly by right ventricular and tricuspid annular dilation [4]. The tricuspid valve has often been the “forgotten valve” during the treatment of left sided valvular lesions, yet the incidence of at least moderate tricuspid insufficiency in patients undergoing mitral valve surgery may be as high as 30% [5]. The clinical determinants of FTR include pulmonary hypertension [6], volume overload [7], and ischemic wall motion abnormalities leading to papillary muscle displacement and leaflet tethering [8]. Reduced myocardial contractility surrounding the tricuspid annulus has also been proposed as an additional mechanism of secondary TR [9]. The results of surgical treatment of FTR are still not satisfactory with up to 20% of patients having moderate or greater recurrent TR after repair [5] and re-operative risk being prohibitively high in many patients [10].

Establishment of a pertinent animal model of right ventricular dysfunction with FTR may facilitate improvement in clinical outcomes by elucidating the pathophysiology of this challenging entity and spurring an evolution of novel repair techniques. Contemporary large animal models of RVF involve pressure or volume overload but rarely consider the tricuspid valve [11]. Similarly, models of pure tricuspid insufficiency are centered around direct surgical or percutaneous damage to the valvular complex components i.e. the leaflets [12,13], subvalvular apparatus [14,15], or tricuspid annulus [16,17]. Mechanical prevention of leaflet coaptation [18] or induction of non-physiological right ventricle flow [19] offer alternative strategies to achieve experimental TR. Although the degree of valvular insufficiency achieved in these models is significant, they are far removed from clinical pathophysiology of FTR centered around RV dysfunction. A clinically pertinent large animal model of right ventricle failure (RVF) and functional tricuspid insufficiency is in yet to be described in the literature.

The aim of the current study was to create and validate a large animal model of RVF with functional tricuspid regurgitation that reflects the clinical condition. Together with clinical parameters describing the changes in the RV and tricuspid annulus, we also sought to assess the model in terms of RV strains.

2. Methods

All animals received humane care in compliance with the Guide for Care and Use of Laboratory Animals. The study protocol was approved by our local Institutional Animal Care and Use Committee.

2.1. Surgical preparation

Sixteen healthy Dorset castrated male sheep had external right jugular intravenous catheter placed under local anesthesia with 1% lidocaine. Animals were then anesthetized with propofol (2–5 mg/kg IV), intubated, and mechanically ventilated. General anesthesia was maintained with inhalational isoflurane (1–2.5%). Fentanyl (5–20 µg/kg/min) was infused as additional maintenance anesthesia. An 18 Ga arterial catheter was introduced through left carotid artery for arterial blood pressure measurements. Animals were fully heparinized and the right internal jugular artery and right internal jugular vein were exposed and cannulated in preparation for cardiopulmonary bypass (CPB). The operative procedure was performed through a sternotomy and the heart was exposed in a pericardial cradle. Pressure transducers (PA4.5-X6; Konigsberg Instruments, Inc., Pasadena, CA, USA) were placed in the LV and RV through the apex. Additional pressure transducer was placed in the right atrium (RA). A 24 mm pulmonary artery pneumatic occluder (In Vivo Metric, Healdsburg, CA, USA) was placed around the main pulmonary artery. Caval snares were placed around the superior and inferior vena cava cannulated with a multi-stage venous cannula via the right jugular vein. After activated clotting time exceeded 480 s, normothermic CPB was initiated. On the beating heart and with both cava snared, the right atrium was opened and six 2 mm sonomicrometry crystals (Sonometrics Corporation, London, Ontario, Canada) were implanted with 5–0 polypropylene suture around the tricuspid annulus. One crystal was implanted at each commissure and an additional crystal equidistant between the commissures. Crystal electrodes were exteriorized through the right atriotomy. Four crystals were implanted on the right ventricular myocardium along the mid right ventricular free wall with a fifth crystal at the right ventricular apex (Fig. 1). An ECG electrode was sutured to the right ventricular free wall. A silastic snare was placed around the posterior descending artery (PDA) branch of the circumflex coronary artery close to the atrio-ventricular groove. After completion of crystal placements, the atriotomy was closed and the animal was weaned from CPB. Animals were allowed to stabilize for 30 min to achieve steady state hemodynamics prior to simultaneous hemodynamic, sonomicrometric, and echocardiographic data acquisition. Every animal received 300 mg of amiodarone IV and was kept on lidocaine IV drip (0.03 mg/kg/min) to prevent ventricular ectopy during the experimental protocol. All animals were studied as open-chest preparations.

2.2. Model development

In the first phase of the study, ten animals (56 ± 6 kg) were utilized to individually test the influence of clinically recognized predictors of RVF and FTR on ovine tricuspid valve insufficiency in a stepwise approach. Initially, baseline data were gathered and then (1) 500 ml of crystalloid solution was given over a period of 2 min, and subsequently, (2) the pulmonary artery occluder was inflated with air to increase maximal right ventricular pressure by at least 50%. The occluder was then deflated for 5 min and the animal allowed to achieve steady state hemodynamic. Last, (3) posterior descending artery (PDA) was occluded for 5 min. Five minutes of stabilization was permitted between all interventions and data captures to assure steady-state hemodynamics as defined by unchanging blood pressure and heart rate. Simultaneous, hemodynamic, sonomicrometry and echocardiographic data were acquired before and after every intervention.

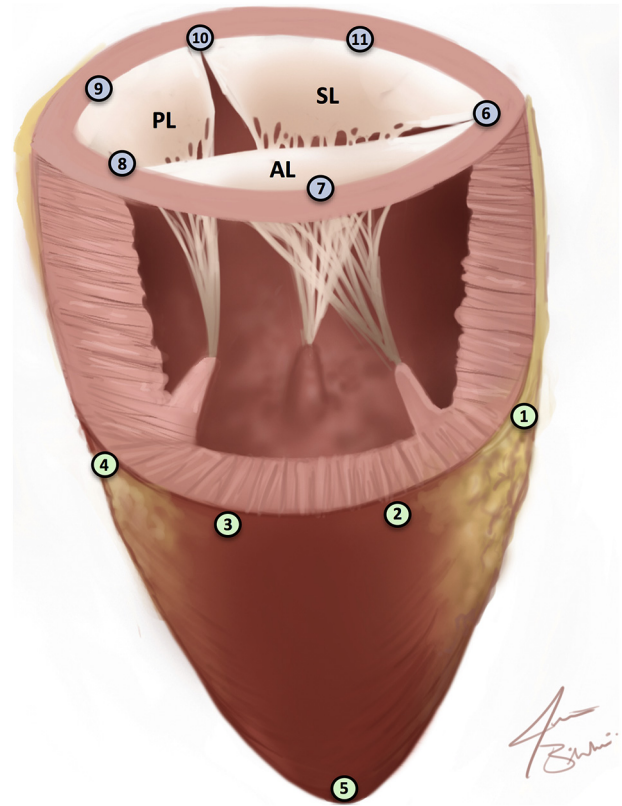


Fig. 1. The location of the sonomicrometry crystals implanted on the right ventricle and around the tricuspid annulus. AL = anterior leaflet, PL = posterior leaflet, SL = septal leaflet.

2.3. Model validation

In the second phase of the experiment, based on the information gathered from the model development series, RVF with FTR was induced in six additional animals (50 ± 2 kg) by the combination of all three interventions tested in the first phase: 500 ml of crystalloid solution bolus infusion over 2 min followed by the occlusion of PDA and subsequent (after 5 min ischemia) pulmonary artery constriction to increase maximal RVP to at least 150% of its pre-occlusion value. The animal was permitted to achieve stable hemodynamics for fifteen minutes under these combined interventions (volume, ischemia, pulmonary hypertension) prior to data collection. Data were collected at baseline and after the combined intervention. At the conclusion of the experiments, the animals were euthanized by administering sodium pentothal (100 mg/kg IV). The heart was excised and the proper placement of annular and ventricular crystals was confirmed.

2.4. Echocardiographic protocol

Epicardial echocardiography was used to acquire all images. It was performed with a 2–4 Mhz transducer connected to a Vivid S6 ultrasound machine (GE Healthcare, USA). The degree of valvular insufficiency was assessed using American Society of Echocardiography criteria. Grading included comprehensive evaluation of color flow and continuous wave Doppler. TR was graded accordingly and categorized by an experienced cardiologist (D.L) as none or trace (0), mild (+1), moderate (+2), moderate to severe (+3) and severe (+4).

2.5. Sonomicrometric data acquisition and analysis

All sonomicrometry data were acquired using a Sonometrics Digital Ultrasonic Measurement System DS3 (Sonometrics Corporation, London, Ontario, Canada) as previously described [20]. Data from ten consecutive cardiac cycles during normal sinus rhythm were averaged for each animal. Data were acquired at 128 Hz with simultaneous LVP, RVP, CVP and ECG recordings. All sonomicrometry recordings were analyzed in CardioSOFT Software ver. 3.4.70 (Sonometrics Corporation). Annular area and perimeter were calculated based on individual 3D crystal positions as previously described [20]. Septo-lateral (S-L) annular dimension was calculated as the distance between crystals #7 and 11; antero-posterior (A-P) annular dimension as the distance between crystals #6 and 9 (Fig. 1).

Sonomicrometry derived RV contraction was calculated as the difference between the end-diastolic and end-systolic area enclosed by crystals #1–4 ($[A_{ED} - A_{ES}] / A_{ED} * 100\%$). RV volume was calculated using convex hull method. The RV radius of curvature (RV ROC)

was calculated based on the least squares approach and fitting a circle to crystals #1–4 [21].

All values were calculated at their maximal and minimal during the cardiac cycle and at end-systole (ES) and end-diastole (ED). End-diastole was defined as the time of the beginning of positive deflection in ECG voltage (R wave) while end-systole (ES) was determined as the time of maximum negative dp/dt of left ventricular pressure.

2.6. Ventricular strain analysis

Right ventricular free wall equatorial strain was calculated based on the 3D position of ventricular crystals (#1–4 as depicted in Fig. 1) using the method previously described [22,23]. Strain, as a relative measure of displacement and thus free wall deformation, is calculated relative to a “reference configuration”. Here, we chose baseline at ED and ES as the reference configurations for the model at ED and ES, respectively. Therefore, strain reflects the deformation of the RV free wall in the model relative to the baseline conditions. Specifically, Green-Lagrange strain was calculated along the free wall for each animal and later displayed on a spline representation of the population averaged RV free wall segment. The global and regional strain patterns of the analyzed mid-level segment of RV free wall were calculated for the entire circumference (crystals #1–4) and the anterior (#1–2), middle (#2–3), and posterior (#3–4) wall by averaging them along the respective regions. Negative or “compressive” strains imply that tissue is compressed, while positive or “tensile” strains imply that tissue is stretched.

2.7. Statistical analysis

Data are presented as mean \pm standard deviation unless otherwise stated. The variables measured in model development series were compared between different individual interventions (volume, pulmonary hypertension, ischemia, model) with repeated measures ANOVA or Friedman repeated measures ANOVA on ranks when normality test failed, and compared to control (Baseline) with Dunnett's post hoc test. In the validation series, experimental parameters before (Baseline) and after development of RVF with FTR (Model) were compared using Students' two-tailed *t*-test for dependent observations. *p* value < 0.05 was always considered significant. SigmaPlot 12.5 Software was utilized for statistical analysis (SYSTAT, San Jose, CA).

3. Results

3.1. Model development

All animals underwent uneventful surgery. The mean CPB time was 85 ± 12 min. No cardiac arrhythmias were observed.

3.1.1. Hemodynamics

Hemodynamic variables before (Baseline) and during every intervention are presented in Table 1. Expected hemodynamic changes were observed with volume infusion and pulmonary artery constriction, but isolated PDA ischemia did not perturb LV or RV hemodynamics.

3.1.2. Echocardiography

Echocardiographic assessment of biventricular function and size are presented in Table 1. Reduced RV ejection fraction (EF) and RV fractional area change (FAC) was seen with every intervention. Both RV and LV EF drop together with right atrial enlargement were observed when FTR was present. Significant dilation of the tricuspid annulus and increase in the major right atrial size was observed with PHT and combined intervention. TR increased significantly with isolated PHT but this increase did not achieve a clinically meaningful level. The combined intervention led to at least moderate FTR in all animals.

3.2. Model validation

3.2.1. Hemodynamics

Based on the data obtained from the model development series, in the validation phase, RVF with functional tricuspid regurgitation was successfully created by combined intervention of volume infusion, PDA ischemia and pulmonary hypertension. Induction of RV dysfunction was associated with an increase in maximal RVP from 23 ± 7 to 42 ± 8 mmHg ($p < 0.001$), RV EDP from 9 ± 3 to 14 ± 7 mmHg ($p = 0.059$) while maximal LVP (83 ± 7 vs. 75 ± 13 mmHg; $p = 0.2$) and LV EDP (16 ± 9 vs. 12 ± 4 mmHg; $p = 0.3$) remained unchanged. CVP increased from 9 ± 3 to 13 ± 5 mmHg ($p = 0.02$). FTR increased from 0.4 ± 0.5 at baseline to 2.5 ± 0.8 ($p < 0.001$). All animals remained with stable

hemodynamics and required no inotropic support for the 15-min observation period after model generation.

3.2.2. Right ventricular geometry and contractility

Systolic and diastolic RV dimensions significantly increased as measured by sonomicrometry. The antero-posterior RV diameter (between crystals #1 and #4) enlarged from 84 ± 3 to 86 ± 2 mm ($p = 0.02$) in end-diastole and from 74 ± 3 to 78 ± 1 mm ($p = 0.04$) in end-systole. Cumulative maximal RV free wall length (the sum of distances between crystals 1–4) increased in the model at ED from 138 ± 9 to 144 ± 10 mm ($p = 0.01$) indicative of free wall dilation. The RV free wall dilated significantly in the anterior (50 ± 4 vs 51 ± 5 mm, $p = 0.02$) and middle part (45 ± 3 vs. 47 ± 4 mm, $p = 0.02$) with no change in the posterior segment (44 ± 7 vs 45 ± 9 mm, $p = 0.16$). The end-systolic distance from RV apex to tricuspid annular plane revealed a tendency toward an increase in the model from 44 ± 6 to 46 ± 5 mm ($p = 0.056$). Sonomicrometry derived RV volumes increased alike from 61 ± 14 ml to 70 ± 16 ml ($p = 0.02$) at ED and from 51 ± 14 to 62 ± 16 ml ($p = 0.01$) at ES. RV contractility dropped from 21 ± 2.6 to $12 \pm 2.3\%$ ($p = 0.02$). RV free wall radius of curvature increased from 36.4 ± 2.5 to 38.2 ± 2.6 mm ($p = 0.005$) at ED and from 33.3 ± 2.1 to 35.7 ± 2.3 mm ($p = 0.006$) at ES.

3.2.3. Right ventricular strains

RV free wall showed significant deformation with the development of myocardial dysfunction. Both systolic and diastolic strain pattern in the model revealed greater strain globally and in all individual segments of the mid RV free wall (Fig. 2).

3.2.4. Tricuspid annular size

Tricuspid annulus enlarged significantly with induction of acute RVF. Maximal area increased by $14 \pm 8\%$ and perimeter by $6 \pm 3\%$ (Table 2). The annular perimeter enlarged uniformly across all segments. Maximal anterior annular perimeter enlarged from 28.9 ± 4.5 to 31.1 ± 4.0 mm ($p = 0.01$) and posterior from 24.7 ± 7.8 to 26.0 ± 7.6 mmHg ($p = 0.004$) while the septal annulus enlarged from 36.8 ± 4.2 to 38.0 ± 3.7 ($p = 0.03$).

4. Discussion

The surgical approach toward functional TR has evolved from a conservative strategy rooted in the belief that it resolves with successful treatment of left heart lesions [24], to a more aggressive approach advocated by current guidelines [25]. Despite introduction of different reparative techniques, mild residual FTR is present in >40% of patients immediately after ring annuloplasty [26] with moderate or greater FTR observed in 14% [27] to 22% [28] of patients less than one week post-operatively. Recurrent FTR rates reach approximately 30% beyond one year after surgery [29,30] underscoring our incomplete understanding of the pathophysiology of this complex clinical entity. Large animal models of valvular pathophysiology provide mechanistic insight [31,32] and spur surgical innovation that ultimately may lead to improved clinical results [33]. The current study introduces a novel large animal model of acute FTR that encompasses RV dysfunction, pulmonary hypertension and volume burden as known clinical determinants of functional tricuspid insufficiency.

Functional TR is predominantly attributed to tricuspid annular dilatation secondary to right ventricular chamber dilation, increased pulmonary or right ventricular pressures, or volume overload. As a primary mechanistic target, mechanical damage to the annulus [16,17] through cuts in the annular tissue has been used to create tricuspid regurgitation, but this approach ignores RV remodeling and does not resemble any stage of clinical FTR. Surgical damage to leaflets [13], chords [34] or papillary muscles [14] cannot be treated as a model of FTR but rather produces regurgitation of organic origin that over time can induce RV and atrial dilation due to volume overload. RV

Table 1
Hemodynamic and echocardiographic parameters according to intervention.

Parameter (n = 10)	Baseline	Volume	PHT	Ischemia	Model	p
HR (min ⁻¹)	90 ± 6	95 ± 14	89 ± 10	88 ± 13	89 ± 12	0.43
LV EDP (mm Hg)	17 ± 10	29 ± 19*	14 ± 7	14 ± 7	12 ± 7	0.02
LV ESP (mm Hg)	91 ± 16	127 ± 22*	92 ± 17	84 ± 21	73 ± 21	<0.001
Max.LVP (mm Hg)	94 ± 16	129 ± 22*	96 ± 15	87 ± 22	81 ± 30*	<0.001
RV EDP (mm Hg)	10 ± 6	16 ± 7*	15 ± 4*	10 ± 4	14 ± 5*	<0.001
RV ESP (mm Hg)	23 ± 3	33 ± 6*	45 ± 11*	25 ± 7	44 ± 11*	<0.001
Max.RVP (mm Hg)	25 ± 3	35 ± 5*	47 ± 10*	27 ± 7	45 ± 12*	<0.001
CVP (mm Hg)	9 ± 6	13 ± 7*	12 ± 7*	10 ± 6	15 ± 9*	0.002
<i>Right heart</i>						
TR grade	0.3 ± 0.5	0.8 ± 0.6	1.3 ± 0.5*	1.0 ± 0.7	2.4 ± 0.8*	<0.001
TV annulus (mm) (dimention)	26 ± 4	27 ± 3	28 ± 3*	24 ± 3	27 ± 4*	<0.001
RV FAC (%)	40 ± 7	41 ± 7	29 ± 10*	31 ± 12*	26 ± 9*	<0.001
RV EF (%)	54 ± 12	35 ± 4*	30 ± 10*	32 ± 10*	24 ± 7*	<0.001
RV ESD (cm)	2.0 ± 0.28	2.2 ± 0.34	2.3 ± 0.46	2.1 ± 0.55	2.4 ± 0.56	0.1
RV EDD (cm)	2.7 ± 0.26	2.9 ± 0.24	2.9 ± 0.44	2.6 ± 0.5	3.0 ± 0.6	0.12
RA major (cm)	3.07 ± 0.59	3.71 ± 0.59*	3.7 ± 0.50*	3.64 ± 0.66*	3.84 ± 0.57*	0.009
RA minor (cm)	2.86 ± 0.62	3.22 ± 0.39	3.07 ± 0.46	2.98 ± 0.34	2.97 ± 0.33	0.5
RAA (cm ²)	7.81 ± 2.58	9.23 ± 3.22	9.41 ± 1.26	8.96 ± 1.38	9.83 ± 1.86	0.12
<i>Left heart</i>						
LV EF (%)	55 ± 6	50 ± 6	49 ± 6	45 ± 9*	43 ± 11*	0.01
LV ESD (cm)	2.65 ± 0.28	3.1 ± 0.46*	2.21 ± 0.27*	2.63 ± 0.56	2.61 ± 0.37	<0.001
LV EDD (cm)	3.58 ± 0.56	3.8 ± 0.14	3.07 ± 0.32*	3.20 ± 0.69	3.01 ± 0.30*	<0.001

p value from RM ANOVA. CVP = central venous pressure, EDD = end diastolic diameter, EDP = end diastolic pressure, EF = ejection fraction, ESD = end systolic diameter, ESP = left ventricular end systolic pressure, FAC = fractional area change, HR = heart rate, LV = left ventricular, Max = maximal, PHT = pulmonary hypertension, RA = right atrium, RAA = right atrial area, RV = right ventricular.

* p < 0.05 vs. Baseline by Dunnett's post hoc test.

remodeling was indeed reported during follow-up recovery in a study utilizing this approach [13]. However, these models have very limited applicability to clinical FTR, whereas the model presented in this study is reliable, easy to reproduce, and incorporates clinically relevant factors.

Annular enlargement seen with patients with RV dysfunction and FTR represents the primary repair target for surgical annuloplasty devices. However, similar to functional mitral regurgitation, the pathogenesis of FTR is not limited to the annulus but represents a sum of more complex geometric perturbation. As such, isolated annular reduction may not be sufficient to provide stable surgical results. According to Dreyfus and Chan [35], FTR is a result of progressive dysfunction and dilatation of the RV that in the initial phase results in annular dilatation subsequently followed by progressive RV dilatation, leaflet tethering, and ultimately TR. This is in fact what was observed during the development of our model. A degree of RV failure was observed with volume

infusion, PDA ischemia, and pulmonary hypertension, but only the combined interventions resulted in sufficient acute RV remodeling to trigger FTR. None of these interventions in isolation induced relevant TR although annular enlargement was noted with volume infusion and PHT. These observations corroborate the proposed complex pathophysiology of FTR [35]. We have previously described the effect of acute pulmonary hypertension on ovine tricuspid valve geometry. Similar to the current study, we did not observe clinically significant TR with pressure overload despite presence of annular enlargement and RVF [20]. Indeed, isolated annular dilatation of up to 40% may not result in significant TR [4]. We observed a 14% annular enlargement in our model which without additional subvalvular dysfunction would not be sufficient to acutely perturb the complex mechanism of TV competence. In the current experiment, PDA occlusion was utilized to induce acute ischemia and resultant RVF and papillary muscle displacement as these two related entities have been shown to contribute to FTR by others [4,36]. Moreover, septal

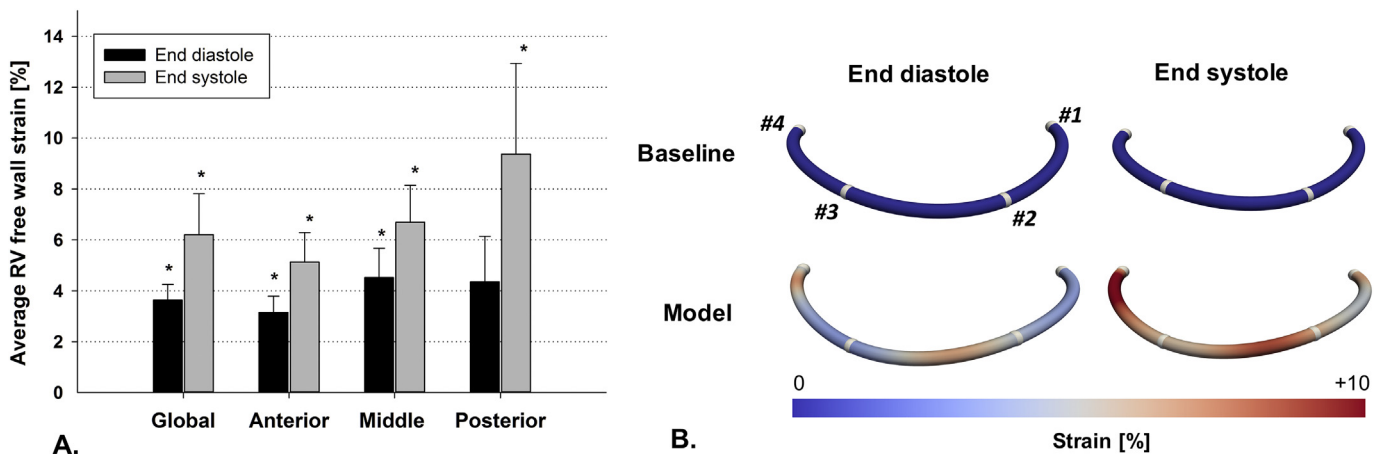


Fig. 2. Right ventricular free wall strain in the model validation group (n = 6). The strain is calculated relative to Baseline condition. *p < 0.05 vs Baseline by means of paired t-test. A) Quantitative average global and regional free wall strain. Error bars indicate 1SEM. B) Color maps of average RV free wall strain. Crystal numbers as depicted in Fig. 1.

Table 2
Tricuspid annular size in model validation.

(n = 6)	Area (mm ²)		Perimeter (mm)		AP diameter (mm)		SL diameter (mm)	
	Baseline	Model	Baseline	Model	Baseline	Model	Baseline	Model
ED	626 ± 102	717 ± 99*	97 ± 7	102 ± 7*	30.1 ± 2.1	31.3 ± 1.6*	25.5 ± 4.4	27.3 ± 3.4*
ES	589 ± 95	668 ± 126*	95 ± 7	100 ± 8*	29.8 ± 2.5	30.4 ± 2.1	23.7 ± 3.5	25.6 ± 3.3*
Max.	652 ± 87	739 ± 87*	99 ± 6	104 ± 5*	31.3 ± 3.3	32.8 ± 2.4*	26.0 ± 3.8	27.8 ± 2.7*
Min.	570 ± 104	649 ± 127*	94 ± 8	99 ± 9*	27.9 ± 2.9	29.0 ± 2.1	23.1 ± 3.8	25.1 ± 3.4*

Data calculated based on sonomicrometric crystals (n = 6). AP = antero-posterior, ED = end-diastole, ES = end-systole, SL = septo-lateral.

* p < 0.05 by paired t-test between Baseline and Model.

ischemia alters interventricular dependence, which is a recognized pathophysiological mechanism of RV dysfunction and subsequent FTR [37]. As we observed lower left ventricular diastolic dimensions with combined interventions, it is feasible that septal shift contributed to the genesis of TR in our model as similar observations were reported by Vargas Abello and colleagues in patients with severe TR [38]. These investigators also found correlation of atrial size and severity of TR. In our model, atrial size increased in the acute setting supporting these clinical observations.

Prior studies suggested that annular dilatation associated with FTR was predominant in the annular segments subtended by the RV free wall [39], but in our model all annular segments enlarged during FTR. Current findings corroborate pig experiments showing that the septal segment is a dynamic structure prone to dilation [40]. However, further studies are needed to describe the geometric and dynamic perturbations in the subvalvular apparatus during FTR.

4.1. Limitations of the study

The results of our study must be interpreted in the context of important limitations. This study did not aim to describe the precise pathophysiology of RVF with FTR. RV dysfunction and tricuspid annular dilation were evident, but we did not assess leaflet tethering nor analyzed in details the changes in subvalvular apparatus. Coronary artery occlusion was utilized to induce RV failure while clinically acute ischemia is not the predominant mechanism responsible for RVF and FTR. The model represents acute RV dysfunction with functional TR and as such is adequate for investigating acute interventions for FTR, but further refinements are needed for chronic applications.

5. Conclusions

In healthy adult sheep, the combination of volume infusion, pulmonary pressure overload, and posterior descending artery ischemia resulted in right ventricular dysfunction and concomitant significant acute functional tricuspid regurgitation. This ovine model embodies right ventricular and tricuspid annular dilation that are representative of clinical functional TR without induction of surgical or mechanical damage to the tricuspid valvular complex. The developed model introduces a reproducible, hemodynamically stable large animal platform to gain better insight into the pathophysiology of right ventricular failure and evaluate novel surgical and interventional approaches.

Acknowledgments

Dr. Malinowski is the Peter C and Pat Cook Endowed Research Fellow in Cardiothoracic Surgery. The authors appreciate the technical assistance provided by Nathan Quay. Authors acknowledge Jeanette Binkowski for the preparation of Fig. 1.

Conflict of interest

The authors report no relationships that could be construed as a conflict of interest.

Funding

Internal grant of Meijer Heart and Vascular Institute at Spectrum Health.

References

- [1] F. Haddad, R. Doyle, D.J. Murphy, S.A. Hunt, Right ventricular function in cardiovascular disease, part II: pathophysiology, clinical importance, and management of right ventricular failure, *Circulation* 117 (2008) 1717–1731.
- [2] F. Haddad, A.Y. Denault, P. Couture, R. Cartier, M. Pellerin, S. Levesque, J. Lambert, J.C. Tardif, Right ventricular myocardial performance index predicts perioperative mortality or circulatory failure in high-risk valvular surgery, *J. Am. Soc. Echocardiogr.* 20 (2007) 1065–1072.
- [3] M. Di Mauro, M. Foschi, F. Tancredi, S. Guarracini, M. Di Marco, A.M. Habib, H. Kheirallah, M. Alsaied, J.J. Alfonso, S. Gallina, A.M. Calafiore, Additive and independent prognostic role of abnormal right ventricle and pulmonary hypertension in mitral-tricuspid surgery, *Int. J. Cardiol.* 252 (2017) 39–43.
- [4] E.M. Spinner, P. Shannon, D. Buice, J.H. Jimenez, E. Veledar, P.J. Del Nido, D.H. Adams, A.P. Yoganathan, In vitro characterization of the mechanisms responsible for functional tricuspid regurgitation, *Circulation* 124 (2011) 920–929.
- [5] B. Mahesh, F. Wells, S. Nashef, S. Nair, Role of concomitant tricuspid surgery in moderate functional tricuspid regurgitation in patients undergoing left heart valve surgery, *Eur. J. Cardiothorac. Surg.* 43 (2013) 2–8.
- [6] D. Mutlak, D. Aronson, J. Lessick, S.A. Reisner, S. Dabbah, Y. Agmon, Functional tricuspid regurgitation in patients with pulmonary hypertension: is pulmonary artery pressure the only determinant of regurgitation severity? *Chest* 135 (2009) 115–121.
- [7] Y. Topilsky, C. Tribouilloy, H.I. Michelena, S. Pislaru, D.W. Mahoney, M. Enriquez-Sarano, Pathophysiology of tricuspid regurgitation: quantitative doppler echocardiographic assessment of respiratory dependence, *Circulation* 122 (2010) 1505–1513.
- [8] S. Fukuda, A.M. Gillinov, J.M. Song, M. Daimon, V. Kongsarepong, J.D. Thomas, T. Shiota, Echocardiographic insights into atrial and ventricular mechanisms of functional tricuspid regurgitation, *Am. Heart J.* 152 (2006) 1208–1214.
- [9] J.B. Barlow, Aspects of tricuspid valve disease, heart failure and the "restriction-dilatation syndrome", *Rev. Port. Cardiol. Orgao Of. Da Soc. Port. Cardiol. Port. J. Cardiol. an Off. J. Port. Soc. Cardiol.* 14 (1995) 991–1004.
- [10] P. Hornick, P.A. Harris, K.M. Taylor, Tricuspid valve replacement subsequent to previous open heart surgery, *J. Heart Valve Dis.* 5 (1996) 20–25.
- [11] M.A.J. Borgdorff, M.G. Dickinson, R.M.F. Berger, B. Bartelds, Right ventricular failure due to chronic pressure load: what have we learned in animal models since the NIH working group statement? *Heart Fail. Rev.* 20 (2015) 475–491.
- [12] P.M. Heerdt, G.A. Blessios, M.L. Beach, C.W. Hogue, Flow dependency of error in the modification measurement of cardiac output during acute tricuspid regurgitation, *J. Cardiothorac. Vasc. Anesth.* 15 (2001) 183–187.
- [13] X.J. Xie, S.J. Liao, Y.H. Wu, C. Lu, P. Zhu, H.W. Fei, X.J. Xiao, H.L. Huang, Tricuspid leaflet resection in an open beating heart for the creation of a canine tricuspid regurgitation model, *Interact. Cardiovasc. Thorac. Surg.* 22 (2016) 149–154.
- [14] H. Hoppe, D. Pavcnik, T.A. Chuter, E. Tseng, M.D. Kim, I. Bernat, B. Uchida, F.S. Keller, J. Röscher, Percutaneous technique for creation of tricuspid regurgitation in an ovine model, *J. Vasc. Interv. Radiol.* 18 (2007) 133–136.
- [15] M.J. Miller, R.G. McKay, J.J. Ferguson, P. Sahagian, S. Nakao, P.C. Come, W. Grossman, Right atrial pressure-volume relationships in tricuspid regurgitation, *Circulation* 73 (1986) 799–808.
- [16] M. Otaki, R.M. Lust, Modification of De Vega's tricuspid annuloplasty for experimental tricuspid regurgitation, *J. Card. Surg.* 9 (1994) 399–404.
- [17] E.M.D. Walter, E.M. Delmo Walter, N.V. Vasilyev, B. Sill, M. Padala, J. Jimenez, A.P. Yoganathan, R. Hetzer, P.J. del Nido, Creation of a tricuspid valve regurgitation model from tricuspid annular dilatation using the cardioport video-assisted imaging system, *J. Heart Valve Dis.* 20 (2011) 184–188.
- [18] T. Kinney, G. Olinger, Acute, reversible tricuspid insufficiency: creation in canine model, *Am. J. Dent.* 260 (1991) H638–41.
- [19] F. Maisano, M. Taramasso, A. Guidotti, A. Redaelli, G.B. Fiore, G. Baroni, P. Patete, O. Alfieri, Simulation of functional tricuspid regurgitation using an isolated porcine heart model, *J. Heart Valve Dis.* 20 (6) (2011) 657–663.
- [20] M. Malinowski, P. Wilton, A. Khaghani, D. Langholz, V. Hooker, L. Eberhart, R.L. Hooker, T.A. Timek, The effect of pulmonary hypertension on ovine tricuspid annular dynamics, *Eur. J. Cardio-Thorac. Surg.* 49 (2016) 40–45.

- [21] V. Pratt, Direct least-squares fitting of algebraic surfaces, *SIGGRAPH Comput. Graph.* 21 (1987) 145–152.
- [22] M.K. Rausch, W. Bothe, J.P.E. Kvitting, J.C. Swanson, N.B. Ingels, D.C. Miller, E. Kuhl, Characterization of mitral valve annular dynamics in the beating heart, *Ann. Biomed. Eng.* 39 (2011) 1690–1702.
- [23] M.K. Rausch, M. Malinowski, P. Wilton, A. Khaghani, T.A. Timek, Engineering analysis of tricuspid annular dynamics in the beating ovine heart, *Ann. Biomed. Eng.* 46 (3) (2018) 443–451.
- [24] N.S. Braunwald, J. Ross, A.G. Morrow, Conservative management of tricuspid regurgitation in patients undergoing mitral valve replacement, *Circulation* 35 (1967) 163–169.
- [25] R.A. Nishimura, C.M. Otto, R.O. Bonow, B.A. Carabello, J.P. Erwin, R.A. Guyton, P.T. O’Gara, C.E. Ruiz, N.J. Skubas, P. Sorajja, T.M. Sundt, J.D. Thomas, *AHA/ACC guideline for the management of patients with valvular heart disease: a report of the American college of cardiology/American heart association task force on practice guidelines*, *J. Am. Coll. Cardiol.* 63 (22) (2014) e57–e185.
- [26] B. Pfannmüller, T. Doenst, K. Eberhardt, J. Seeburger, M.A. Borger, F.W. Mohr, Increased risk of dehiscence after tricuspid valve repair with rigid annuloplasty rings, *J. Thorac. Cardiovasc. Surg.* 143 (2012) 1050–1055.
- [27] P.M. McCarthy, S.K. Bhudia, J. Rajeswaran, K.J. Hoercher, B.W. Lytle, D.M. Cosgrove, E.H. Blackstone, S.F. Bolling, A.F. Carpentier, N.G. De Vega, K.D. Accola, R. Seitelberger, G.D. Dreyfus, Tricuspid valve repair: durability and risk factors for failure, *J. Thorac. Cardiovasc. Surg.* 127 (2004) 674–685.
- [28] S. Fukuda, J.M. Song, A.M. Gillinov, P.M. McCarthy, M. Daimon, V. Kongsarepong, J.D. Thomas, T. Shiota, Tricuspid valve tethering predicts residual tricuspid regurgitation after tricuspid annuloplasty, *Circulation* 111 (2005) 975–979.
- [29] T.T. Ton-Nu, R.A. Levine, M.D. Handschumacher, D.J. Dorer, C. Yosefy, D. Fan, L. Hua, L. Jiang, J. Hung, Geometric determinants of functional tricuspid regurgitation: insights from 3-dimensional echocardiography, *Circulation* 114 (2006) 143–149.
- [30] K. Onoda, F. Yasuda, M. Takao, T. Shimono, K. Tanaka, H. Shimpō, I. Yada, Long-term follow-up after Carpentier-Edwards ring annuloplasty for tricuspid regurgitation, *Ann. Thorac. Surg.* 70 (2000) 796–799.
- [31] F.A. Tibayan, Geometric distortions of the mitral valvular-ventricular complex in chronic ischemic mitral regurgitation, *Circulation* 108 (2003) 11611–121.
- [32] T.A. Timek, P. Dagum, D.T. Lai, D. Liang, G.T. Daughters, N.B. Ingels, D.C. Miller, Pathogenesis of mitral regurgitation in tachycardia-induced cardiomyopathy, *Circulation* 104 (12 Suppl 1) (2001) 147–1153.
- [33] F. Langer, T. Kunihara, K. Hell, R. Schramm, K.I. Schmidt, D. Aicher, M. Kindermann, H.J. Schäfers, RING+STRING successful repair technique for ischemic mitral regurgitation with severe leaflet tethering, *Circulation* 120 (2009) S85–S91.
- [34] N. Minato, T. Itoh, Direct imaging of the tricuspid valve annular motions by fiberoptic cardioscopy in dogs with tricuspid regurgitation. II. Does flexible ring annuloplasty preserve the annular motions? *J. Thorac. Cardiovasc. Surg.* 104 (1992) 1554–1560.
- [35] G.D. Dreyfus, K.M.J. Chan, Functional tricuspid regurgitation: a more complex entity than it appears, *Heart* 95 (2009) 868–869.
- [36] H. Yamauchi, N.V. Vasilyev, G.R. Marx, H. Loyola, M. Padala, A.P. Yoganathan, P.J. Del Nido, Right ventricular papillary muscle approximation as a novel technique of valve repair for functional tricuspid regurgitation in an ex vivo porcine model, *J. Thorac. Cardiovasc. Surg.* 144 (2012) 235–242.
- [37] N.F. Voelkel, R.A. Quaife, L.A. Leinwand, R.J. Barst, M.D. McGoon, D.R. Meldrum, J. Dupuis, C.S. Long, L.J. Rubin, F.W. Smart, Y.J. Suzuki, M. Gladwin, E.M. Denholm, D.B. Gail, Right ventricular function and failure: report of a National Heart, Lung, and Blood Institute working group on cellular and molecular mechanisms of right heart failure, *Circulation* 114 (2006) 1883–1891.
- [38] L.M. Vargas Abello, A.L. Klein, T.H. Marwick, E.R. Nowicki, J. Rajeswaran, S. Puwanant, E.H. Blackstone, G.B. Pettersson, Understanding right ventricular dysfunction and functional tricuspid regurgitation accompanying mitral valve disease, *J. Thorac. Cardiovasc. Surg.* 145 (5) (2013) 1234–1241.
- [39] G.D. Dreyfus, P.J. Corbi, K.M.J. Chan, T. Bahrami, Secondary tricuspid regurgitation or dilatation: which should be the criteria for surgical repair? *Ann. Thorac. Surg.* 79 (2005) 127–132.
- [40] H. Fawzy, K. Fukamachi, C.D. Mazer, A. Harrington, D. Latter, D. Bonneau, L. Errett, Complete mapping of the tricuspid valve apparatus using three-dimensional sonomicrometry, *J. Thorac. Cardiovasc. Surg.* 141 (2011) 1037–1043.